Article

Not peer-reviewed version

Experimental and Numerical Investigation into Active–Passive Behavior and Shear Resistance of Anchored Rock Joints

Yinfeng Tang *, Tongxu Wang , Yuxiang Ma , Yaling Wang

Posted Date: 3 June 2026

doi: 10.20944/preprints202606.0283.v1

Keywords: anchored rock joints; active–passive behavior; shear resistance; direct shear test; failure mode

 doi:10.20944/preprints202606.0283.v1

Article

Experimental and Numerical Investigation into Active–Passive Behavior and Shear Resistance of Anchored Rock Joints

Yinfeng Tang [1,*], Tongxu Wang [2], Yuxiang Ma [1] and Yaling Wang [1]

[1] School of Architectural Environment, Ningxia Institute of Science and Technology, Shizuishan 753000, China

[2] College of Energy and Mining Engineering, Shandong University of Science and Technology, Qingdao 266590, China

* Correspondence: tyf2143655@163.com; Tel.: +86-152-1648-1795

Featured Application

This work provides a theoretical basis and practical reference for the stability analysis and design of anchored jointed rock masses in geotechnical engineering.

Abstract

To elucidate the active–passive reinforcement mechanisms of rock bolts and the evolution of shear strength in anchored rock joints, this study integrates theoretical analysis, laboratory direct shear tests, and numerical simulations to investigate the deformation and failure characteristics of fully grouted, end-anchored, and prestressed bolted specimens. The results show that bolt reinforcement can be classified into prestress-dominated active action and dislocation-induced passive action. The shear strength curve of anchored rock joints exhibits four distinct stages with increasing shear displacement: initial slip, elasticity, yielding, and softening. Fully grouted bolts fail primarily by tensile–shear fracture, enabling a rapid increase in shear strength at small displacements. In contrast, end-anchored bolts undergo S-shaped bending and form plastic hinges; although their anti-sliding efficiency declines under large displacements, they continue to provide sustained resistance. For prestressed bolts, the active contribution accounts for approximately 69.6% of the total shear strength enhancement, while the passive contribution is about 30.4%. These mechanisms act synergistically to improve the shear resistance of rock joints and effectively control early-stage deformation of the surrounding rock. The findings offer a theoretical basis and experimental support for the support design and stability evaluation of rock anchoring projects, such as slopes and tunnels.

Keywords: anchored rock joints; active–passive behavior; shear resistance; direct shear test; failure mode

1. Introduction

Rock bolts, as a critical support technology, are extensively utilized for the stabilization and reinforcement of rock masses in engineering fields such as slopes, underground caverns, and mining roadways [1–3]. Rock joints, acting as inherent weak zones within rock masses, compromise integrity and continuity. They are the primary triggers for engineering disasters, including slope instability, tunnel collapse, and surrounding rock slippage in stopes [4,5]. In practical engineering, the deformation direction of the surrounding rock often deviates from the axial direction of the bolt. Particularly when rock joints are developed, bolts are subjected to coupled axial tension and transverse shear loads, rendering them susceptible to tensile-shear fracture or bending yield. Such failures can lead to the loss of support effectiveness and subsequent engineering hazards [6,7].

 doi:10.20944/preprints202606.0283.v1

Therefore, elucidating the mechanism by which bolts enhance the shear strength of rock joints and its evolution law holds significant practical importance.

The enhancement of shear strength provided by bolts is essentially governed by the manner in which stress is generated. Existing studies categorize this effect into active action and passive action. Active action originates from the application of prestress, providing an initial shear resistance prior to rock joints dislocation, thereby controlling early-stage deformation. Conversely, passive action is induced by the dislocation of the rock joints itself, further enhancing shear capacity through localized stress concentration and deformation responses of the bolt. Ge et al. [8] established a theoretical formula for the shear strength of bolted rock joints, clarifying the contributions of the bolt dowel effect and axial force conversion. Ferrero [9] experimentally revealed the influence of rock mass strength on bolt failure modes. Regarding experimental investigations, direct shear tests on anchored specimens with rock joints under various working conditions have been conducted to explore shear performance and mechanisms [10–13]. In terms of numerical simulation, modifications to FLAC3D elements have been implemented to simulate the tensile-shear coupled failure of bolts [14–20].

However, current research predominantly focuses on fully grouted conditions. There remains a notable lack of understanding regarding the mechanism when rock joints are located within the free segment of the bolt. Furthermore, the synergetic evolution law and quantitative contribution analysis of active-passive actions are insufficient, and the dynamic correlation between the local deformation range of the bolt and the shear displacement of the rock joints remains unclear.

To address these gaps, this study adopts a combined methodology of theoretical analysis, laboratory direct shear tests, and numerical simulations. It systematically investigates the deformation and failure characteristics of bolts under fully grouted, end-anchored, and prestressed conditions. The study aims to quantify the synergistic contribution of active and passive actions and reveal the evolution law of shear strength in anchored rock joints.

2. Theoretical Analysis of Load Transfer Mechanisms in Anchored Rock Joints

2.1. Classification of Active and Passive Strength Enhancement Stages

Based on the origin of stress generation within the bolt, the reinforcement effect is classified into active action and passive action. Active action refers to the enhancement of shear strength induced by bolt pre-stress prior to any displacement. Passive action refers to the enhancement induced by the dislocation of the rock joints itself. As the rock joint dislocates, the shear strength curve can be divided into four distinct stages: initial slip, elastic stage, yielding stage, and softening stage, as illustrated in Figure 1.

1. Initial Slip Stage

During the initial slip stage, the shear stress increases rapidly, manifesting as a near-vertical linear segment on the stress-displacement curve. The height of this segment is determined by both the inherent shear strength of the rock joints and the magnitude of the bolt pre-stress. At this point, due to the minimal shear displacement, local deformation of the bolt at the rock joint location has not yet occurred. Consequently, the pre-stress in the bolt exerts an active supporting role, elevating the shear strength of the rock joints.

2. Elastic Stage

As the shear displacement increases, local deformation begins to develop in the bolt near the rock joints. The bolt remains in an elastic state, and the shear strength curve enters the elastic stage. During this phase, the shear strength increases rapidly. Since this enhancement is triggered by the relative displacement of the rock joints, the bolt functions passively to improve the shear resistance.

3. Yielding Stage

With continued displacement, the bolt undergoes bending yield. The shear strength curve enters the yielding stage, characterized by a deceleration in the growth rate of the slope until it stabilizes. The onset of yielding is influenced by three factors: the yield strength of the bolt, the strength of the

 doi:10.20944/preprints202606.0283.v1

surrounding rock, and the anchorage method. Specifically, a higher bolt yield strength leads to a larger shear displacement at the yielding point. Conversely, weaker rock mass properties result in a larger displacement required to reach yielding. Regarding anchorage methods, bolts with a free segment at the rock joints exhibit yielding at larger displacements compared to those with a fully grouted segment.

4. Softening Stage

With further dislocation, the asperities on the rock joints are flattened, sheared off, and crushed into fine powder. This process weakens the friction coefficient of the joint. Consequently, the normal force component converted from the bolt's tensile axial force diminishes, leading to a decline in the shear stress curve.

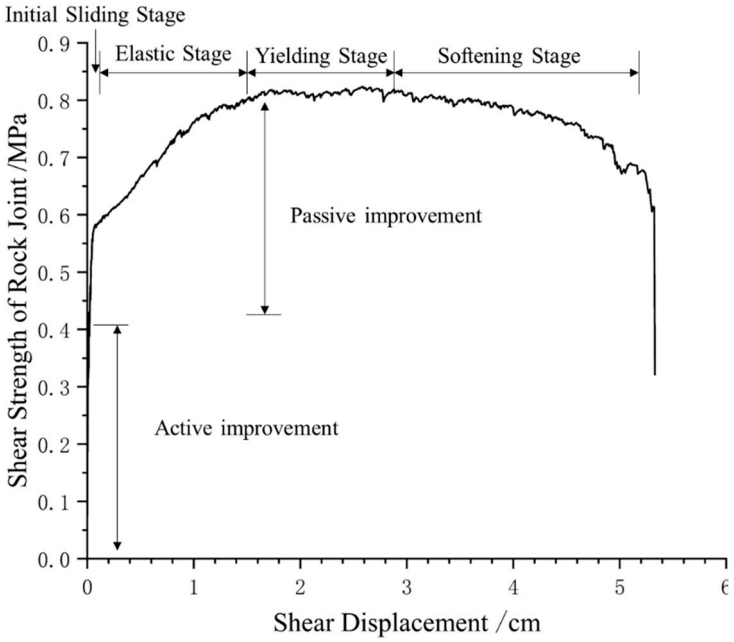

Figure 1. Shear strength variation of bolted rock joints.

In summary, the primary characteristic of active action is the provision of immediate shear strength prior to rock joints movement, effectively controlling early-stage dislocation. In contrast, passive action is characterized by the increase in bolt axial force resulting from local deformation caused by ongoing dislocation, thereby continuously enhancing shear strength as the displacement progresses.

2.2. Calculation of Shear Strength Improvement of Rock Joints by Bolt Active and Passive Actions

Ge Xiurun et al. [8] proposed the calculation formula for the shear strength of anchored rock joints, as expressed in Equation (1). According to this model, the shear strength of the rock joints (τ_{bj}) comprises four distinct components: the inherent shear strength of the rock joints itself (τ_j), the contribution from the dowel action of the bolt body (τ_{bd}), the contribution induced by the normal component of the bolt axial force (τ_{bi}), and the contribution induced by the tangential component of the bolt axial force (τ_{bs}).

$$\tau_{bj} = \tau_j + \tau_{bd} + \tau_{bi} + \tau_{bs} \quad (1)$$

Building upon Equation (1), the passive enhancement of shear strength induced by rock joints dislocation is considered. This effect is quantified by the additional axial stress ($\Delta\sigma$) generated in the bolt, as defined by the following equations:

 doi:10.20944/preprints202606.0283.v1

$$\tau_j = C_j + \sigma_j \tan \varphi_j \quad (2)$$

$$\tau_{bd} = \tau_b \cdot \eta \left(\sin \alpha - \cos \alpha \cdot \tan \varphi_j \right) \quad (3)$$

$$\tau_{bi} = (\sigma_b + \Delta\sigma) \sin \alpha \cdot \tan \varphi_j \cdot \eta \quad (4)$$

$$\tau_{bs} = (\sigma_b + \Delta\sigma) \cos \alpha \cdot \eta \quad (5)$$

With the dislocation of the rock joints, the force condition of the bolt is shown in Figure 2. Among these parameters:

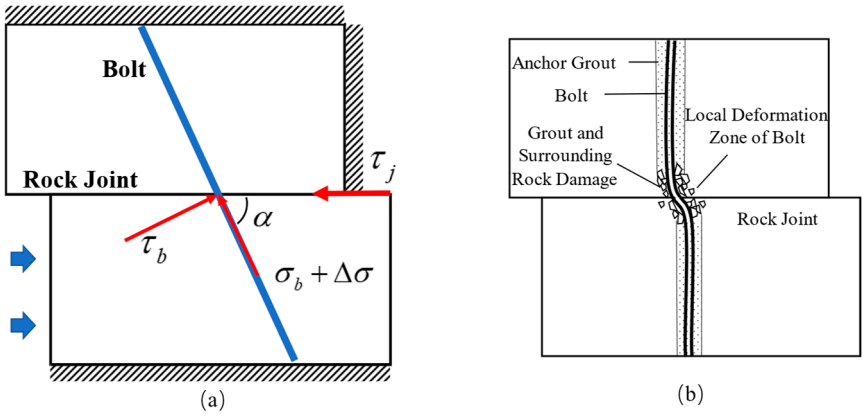

Figure 2. Schematic diagram of bolt reinforcement mechanism acting on the rock joints. (a) Macro-mechanical model showing the force state; (b) Micro-damage model showing grout and bolt deformation.

σ_b : Axial stress of the bolt at the rock joints (tensile stress is positive);

τ_b : Shear stress of the bolt at the rock joints;

$\Delta\sigma$: Incremental axial stress of the bolt induced by the dislocation of the rock joints;

σ_j : Normal stress of the rock joints;

C_j : Cohesion of the rock joints;

φ_j : Friction angle of the rock joints;

α : Bond angle of the bolt (defined as the angle between the shear displacement direction of the rock joints and the bolt on the same side);

η : Ratio of the cross - sectional area of a single bolt to the area of the rock joints.

The increment of shear strength of the rock joints caused by the bolt action, $\Delta\tau_j$, is:

$$\Delta\tau_j = \tau_{bd} + \tau_{bi} + \tau_{bs}$$

The passive enhancement of the rock joints shear strength by the bolt is provided by the incremental axial stress $\Delta\sigma$ generated after the bolt undergoes local deformation, which is reflected in τ_{bi} and τ_{bs}.

2.3. Failure Modes and Stress Evolution Laws of Bolts

When a rock joint dislocates, two primary failure modes may occur at the bolt location: shear failure and bending failure.

Case 1: Bolt Shear Fracture

Shear failure occurs when the local damage to the grout at the rock joints is negligible or very limited. In this scenario, as the surrounding rock displaces, shear forces dominate, leading to the direct cutting of the bolt shank, as illustrated in Figure 3.

Case 2: Bolt Bending Yield

 doi:10.20944/preprints202606.0283.v1

Bending yield occurs with increasing shear displacement, accompanied by progressive damage to the grout near the rock joints. When the damage range of the grout reaches or exceeds 5d (where dis the bolt diameter), plastic hinges form on both sides of the rock joints, as shown in Figure 3. At this stage, further dislocation does not increase the shear strength of the rock joints, indicating that the bolt has reached its limit state and is considered to have failed.

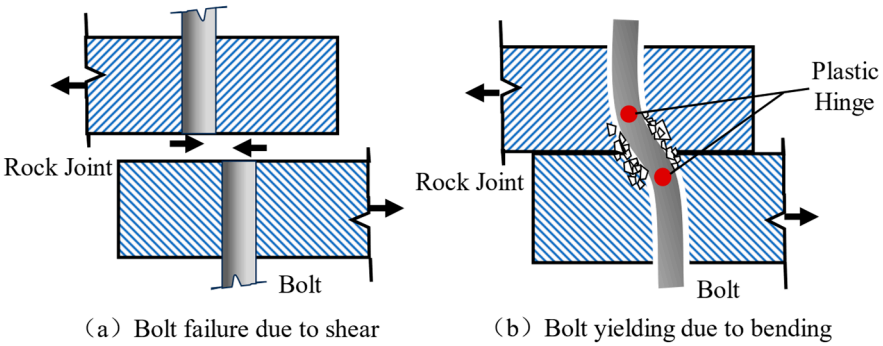

Figure 3. Failure modes of bolts at rock joints: (a) shear failure, where the bolt is fractured across the rock joints; (b) bending yield, where a plastic hinge is formed in the bolt due to bending deformation.

It can be concluded that the failure mode of the bolt is critically dependent on the constraint condition at the rock joints. A limited constraint range typically results in shear fracture, whereas a substantial constraint range leads to bending yield; this constraint is governed by factors such as grout damage length, rock strength, dislocation magnitude, and anchorage method. Based on the origin of stress generation, the bolt's reinforcement effect is classified into active action and passive action. Active action, driven by pre-stress, provides an initial shear strength prior to rock joints movement, effectively suppressing early-stage dislocation. In contrast, passive action is triggered by the dislocation-induced local deformation of the bolt, which increases the bolt stress to enhance shear resistance. The defining characteristic of passive action is the progressive increase in shear strength with accumulating shear displacement.

3. Laboratory Direct Shear Testing of Anchored Rock Joints

3.1. Specimen Fabrication and Design of Anchorage Parameters

To investigate the variation law of shear stress in anchored rock joints under rock mass dislocation, the similarity ratio method was adopted to select materials for the bolts, grouting agents, and rock masses, ensuring the test results align with actual engineering conditions. Based on common engineering support parameters—a borehole diameter of 32 mm, a bolt diameter of 20 mm, and a bolt spacing of 800 mm × 800 mm—this study defined the anchorage prototype. Using a geometric similarity ratio of 8:1, the specimen dimensions were calculated as 100 mm × 100 mm × 80 mm (Length × Width × Height). Accordingly, the borehole diameter was scaled to 4 mm and the bolt diameter to 2.5 mm. Magnesium-aluminum alloy rods were selected as the bolt bodies, fastened using M3 washers and M3 nuts. The mechanical parameters of the bolt material are summarized in Table 1.

Table 1. Mechanical parameters of bolt material.

Material	Drilling Diameter / mm	Bolt Diameter / mm	Elastic Modulus / GPa	Poisson's Ratio	Yield Strength / MPa	Tensile Strength MPa
HRB335	32	20	200	0.3	335	455
Aluminum-Magnesium Alloy	4	2.5	69.3	0.33	195	230

 doi:10.20944/preprints202606.0283.v1

In conventional engineering practice, cement mortar or resin is typically utilized as the grouting agent. However, given the small borehole diameter of 4 mm in this experiment, cement mortar was deemed impractical for effective anchorage. Consequently, an epoxy-based rebaring adhesive was selected as the grouting agent for this study. This adhesive is formulated from two components: modified epoxy resin and a curing agent, mixed at a 1:1 ratio according to standard engineering configurations. The mechanical parameters of the selected grouting agent are presented in Table 2.

Table 2. Mechanical parameters of anchoring agent.

Material	Compressive Strength / MPa	Tensile Strength / MPa	Elastic Modulus / GPa	Poisson's Ratio	Cohesion / MPa	Friction Angle / °
Anchoring Agent	28.25	4.38	1.78	0.12	6.40	16.5

In similitude theory, the stress similarity ratio is typically 1.5 times the geometric similarity ratio; thus, for this study, the stress similarity ratio for the rock-like specimens was set to 12:1. Considering the failure characteristics of the rock joints, the stability of mechanical properties, and the ease of fabrication, high-strength gypsum powder was selected as the modeling material and prepared at a mass ratio of 1:0.4 (gypsum powder to water). Uniaxial compression tests and Brazilian splitting tests were conducted to determine the mechanical properties of the gypsum specimens, as summarized in Table 3. To obtain the shear parameters of the prefabricated rock joints, direct shear tests were performed under various normal stresses. Through linear fitting of the test data, the cohesion (C_j) of the gypsum rock joints was determined to be 0.0233 MPa, with an internal friction angle (φ_j) of 35.16°.

Table 3. Comparison of basic mechanical parameters between rock-like materials and sandstone.

Material	Compressive Strength / MPa	Tensile Strength / MPa	Elastic Modulus / GPa	Poisson's Ratio	Cohesion / MPa	Friction Angle / °
Sandstone	20~170	2~25	3~35	0.1~0.3	1~40	25~60
Rock-like Material	1.67~14.17	0.17~2.08	0.25~2.92	0.1~0.3	0.0833~3.33	25~60
Gypsum Specimen	13.12	1.82	1.87	0.28	0.085	48

Two anchorage scenarios were investigated in this study: fully grouted anchorage and end-anchorage, as illustrated in Figure 4. For the fully grouted specimens, the borehole was first filled with epoxy-based rebaring adhesive, followed by the insertion of the bolt, installation of the washer, and tightening of the nut. For the end-anchored specimens, the bolt was inserted directly into the borehole without filling the entire hole, and then the washer was installed and the nut was tightened to secure the bolt.

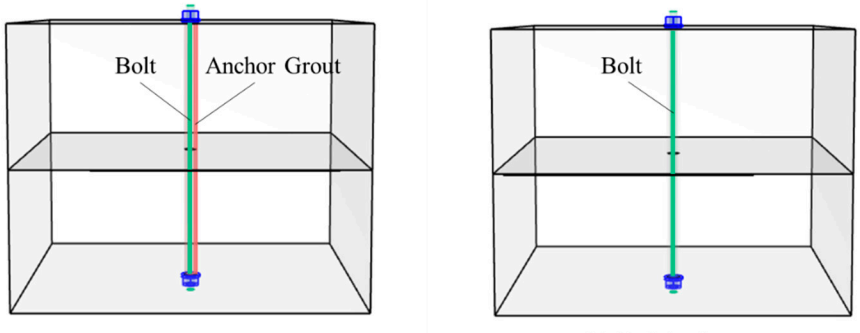

(a) Fully Bonded Anchorage (b) End Anchorage

 doi:10.20944/preprints202606.0283.v1

Figure 4. Schematic diagram of specimens with different anchoring conditions.

3.2. Experimental Scheme Design

The direct shear tests were conducted using an RLJW-2000 microcomputer-controlled rock servo triaxial and shear testing machine. The horizontal shear loading system and the vertical loading system were employed to apply loads to the specimens. During the test, the specimen was placed into the horizontal shear stress loading system with the rock joints oriented vertically, as shown in Figure 5. The horizontal direction of the specimen was constrained, while the vertical direction was loaded.

Figure 5. Test system and loading method.

The detailed experimental procedure was as follows:

1. Preheating and Inspection: The testing machine was preheated, and the indicators of all sensors were checked to ensure they were within the normal operating range.
2. Specimen Protection: Before placing the specimen, steel plates with pre-drilled holes were positioned on the left and right sides of the specimen. The portion of the bolt extending out of the specimen was inserted into the holes of the steel plates to prevent damage to the ends of the anchored specimen during loading.
3. Sensor Setup: Horizontal and vertical displacement sensors were arranged appropriately, and their positions were adjusted to ensure normal readings.
4. Horizontal Confinement: A horizontal stress of 0.05 MPa was first applied to fix the specimen. Once the horizontal stress reached the predetermined value, it was maintained as a constant.
5. Vertical Loading: The vertical loading rate was set to 0.3 mm/min, with a maximum displacement observation limit of 12 mm.
6. Data Acquisition: Real-time shear data were recorded by computer. The test was terminated and unloaded once the shear stress-shear displacement curve showed a peak or the bolt fractured.
7. Documentation: Photographic records of the specimens were taken during the test, and all data were preserved for subsequent analysis.

During the shearing process, the vertical load and displacement, along with the horizontal load, were monitored to obtain the variation curve of the shear strength of the rock joints. The enhancement of shear strength provided by the bolt was calculated using Equation (6).

$$\Delta\tau = \tau - \tau_j = \tau - (C_j + \sigma_j \tan\varphi_j) \quad (6)$$

 doi:10.20944/preprints202606.0283.v1

where $\Delta\tau$ is the increment of shear strength enhanced by the bolt, and τ is the total shear strength monitored during the test. The definitions of C_j, φ_j, and σ_j are consistent with those provided in Section 1.2.

3.3. Shear Mechanical Characteristics of Specimens Under Fully Grouted and End-Anchored Conditions

3.3.1. Failure Characteristics of Fully Grouted Bolts

Under fully grouted conditions, the variation curve of the rock joints shear stress with dislocation is shown in Figure 6. It can be observed that the shear stress curve can be divided into three distinct stages:

1. Initial Stage: The shear stress increases sharply with shear displacement, exhibiting a steep slope.
2. Strengthening Stage: Compared to the initial stage, the growth rate of shear stress slows down, showing a relatively reduced slope.
3. Failure Stage: The bolt within the rock joints fractures, leading to a rapid drop in shear stress. The residual shear stress corresponds to the inherent shear strength of the rock joints (τ_j). At this point, the increment of shear strength provided by the bolt ($\Delta\tau$) is quantified as the difference between the peak stress and τ_j.

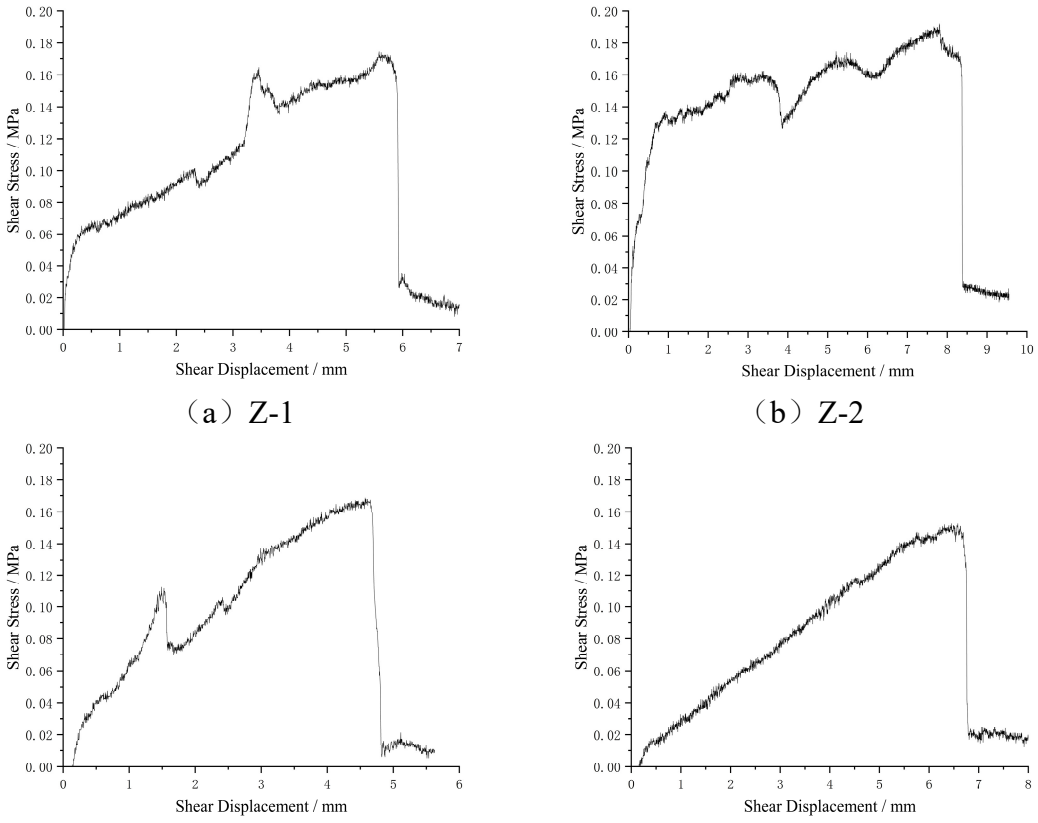

（a）Z-1　（b）Z-2

（c）Z-3　（d）Z-4

 doi:10.20944/preprints202606.0283.v1

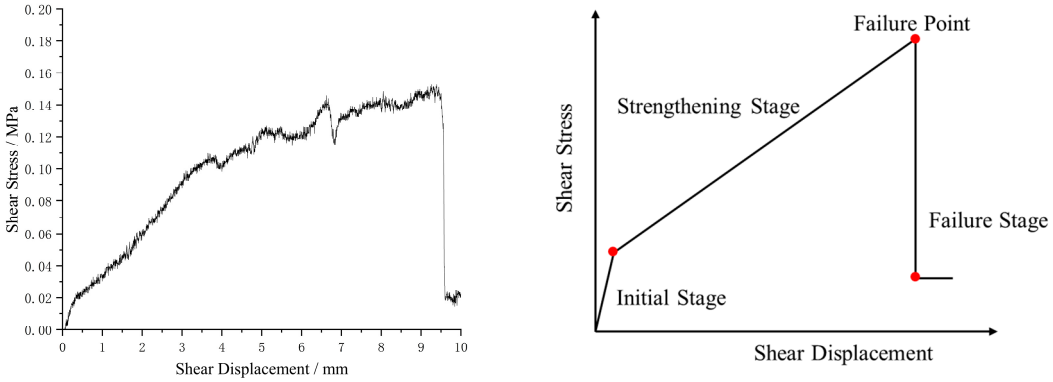

（e）Z-5　　（f）Schematic diagram of shear stress variation

Figure 6. The variation curve of shear stress of rock joint under full anchor condition.

With the dislocation of the rock joints, damage to the surrounding rock and grout near the joint releases the constraint on the bolt, subjecting it to a tensile-shear coupled stress state and ultimately leading to tensile-shear fracture. As illustrated in Figure 7, Specimens Z-1, Z-3, Z-4, and Z-5 exhibited smooth and flat fracture surfaces, indicative of shear-dominated tensile-shear fracture. In contrast, Specimen Z-2 fractured near the bolt end with evident necking, indicating tension-dominated tensile-shear fracture. The lengths of the local deformation zones for these five specimens were 3.72 mm, 10.95 mm, 6.33 mm, 5.89 mm, and 11.13 mm, respectively. Notably, as the fracture of Z-2 occurred outside the rock joints deformation zone, it was treated as an outlier and excluded from the statistical analysis. Based on the remaining four groups, the average length of the local deformation zone was calculated to be 6.7675 mm.

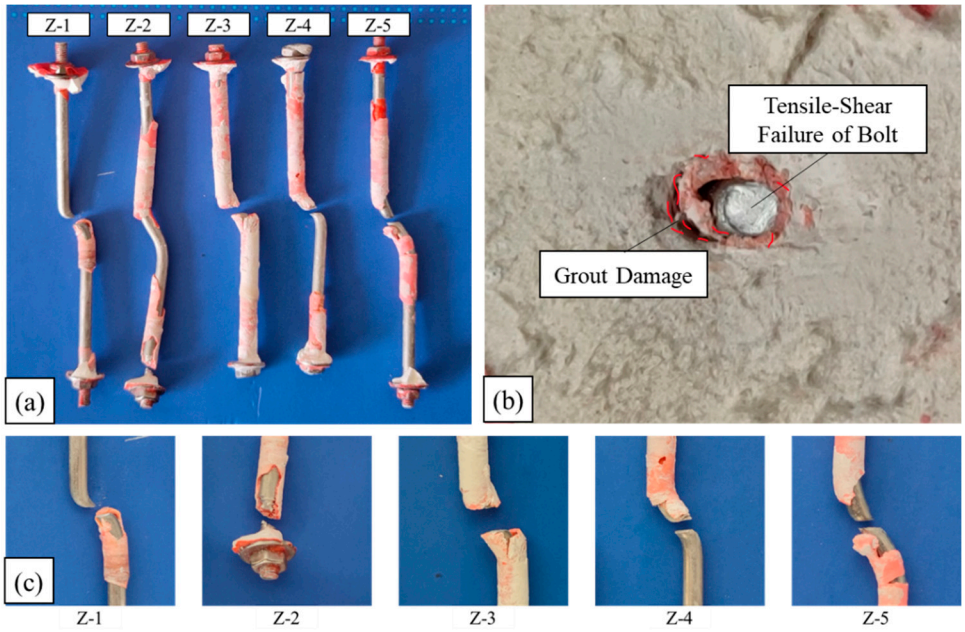

Figure 7. Failure characteristics of fully grouted bolts at rock joints: (a) overall failure modes of bolts in the fully anchored condition; (b) localized tensile-shear fracture of the bolt at the rock joints; (c) detailed views of the bolt fracture morphology.

3.3.2. Failure Characteristics of End-Anchored Bolts

Under end-anchored conditions, the variation curve of the rock joints shear stress with dislocation is shown in Figure 8. Unlike the fully grouted specimens, the shear stress curve exhibits only two stages:

 doi:10.20944/preprints202606.0283.v1

1. Elastic Stage: The shear stress increases linearly with shear displacement, characterized by a relatively steep slope.
2. Yielding Stage: The shear stress stabilizes and maintains a constant value despite continued dislocation of the rock joints.

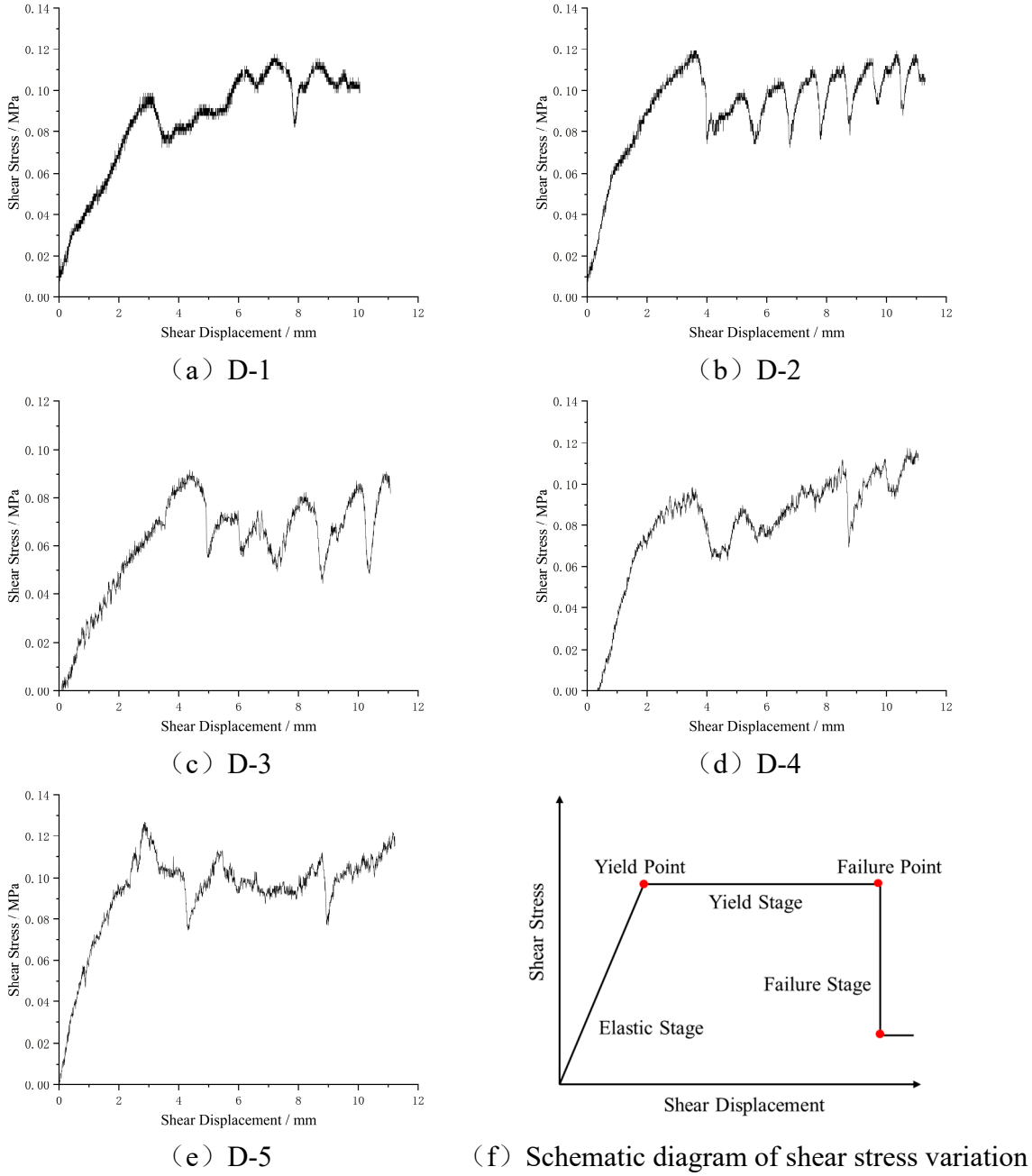

Figure 8. The change curve of shear stress of rock joint under end-anchored.

The deformation characteristics of the end-anchored bolts are shown in Figure 9. The deformation is primarily concentrated near the rock joints, manifesting as an S-shaped bending pattern, with the failure mode identified as bending yield and the formation of two symmetrical plastic hinges on either side of the plane. Compared to fully grouted bolts, the deformation zone at the rock joints is significantly larger. For specimens D-1 to D-5, the bending rotation angles were measured as 51°, 54°, 48°, 50°, and 59°, respectively, while the corresponding distances between the plastic hinges were 9.78 mm, 8.12 mm, 11.03 mm, 10.91 mm, and 7.21 mm. During bending yield, the bolt segment between the plastic hinges undergoes tensile deformation, exhibiting evident necking along the bolt shank.

 doi:10.20944/preprints202606.0283.v1

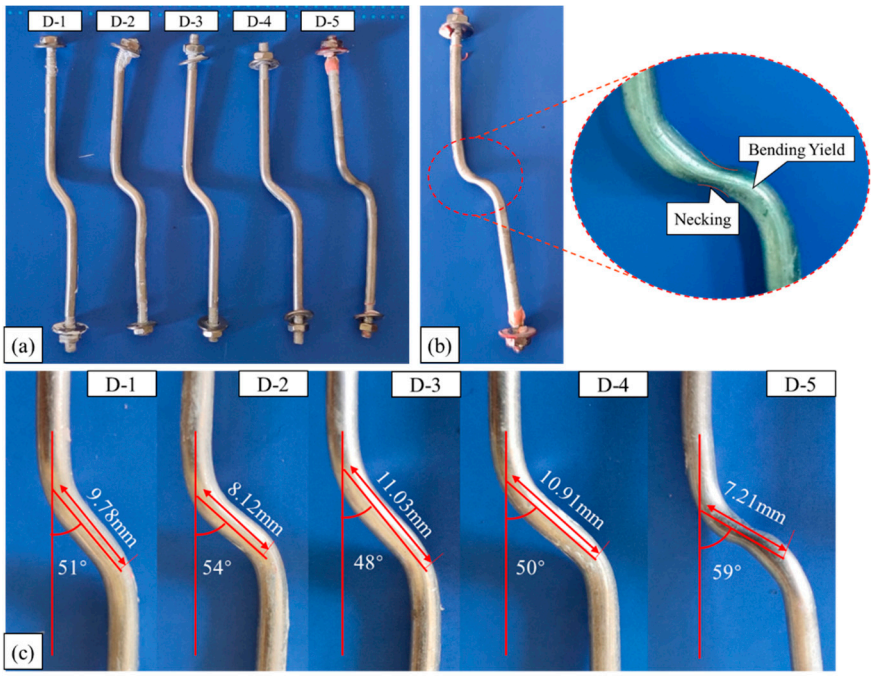

Figure 9. Failure form of end-anchored bolt: (a) bending failure mode of the bolt; (b) necking phenomenon at the bending yield section; (c) detailed views of the bent regions with specific dimensions.

Under end-anchored conditions, a gap exists between the bolt and the borehole wall, leaving the bolt initially unconstrained. As the rock joints begins to dislocate, the surrounding rock comes into contact with one side of the bolt when the shear displacement reaches 1 mm (Figure 12a), initiating bolt deformation under shear. With continued dislocation beyond 2 mm, the bolt contacts the rock mass on the opposite side of the joint (Figure 12b). Given that the bolt stiffness is significantly higher than that of the rock mass, damage occurs at the contact points, forcing the bolt to bend locally near the rock joints and manifest as bending yield with pull-out failure characteristics. If the dislocation continues until the bolt reaches its plastic limit, it would fracture, causing the shear stress to drop to the residual strength (τ_j). However, due to the 12 mm displacement limit of the RLJW-2000 testing machine, the test was terminated upon reaching this maximum stroke; consequently, only the yielding stage of the bolt was captured in this study.

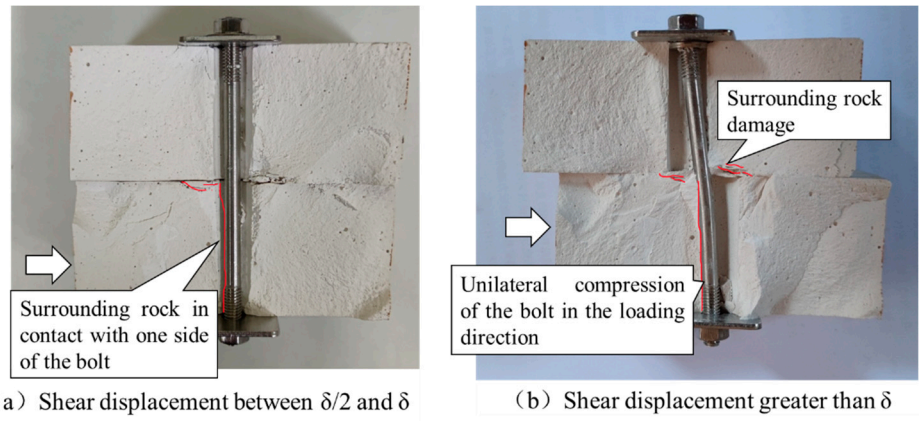

Figure 10. Mechanical behavior of end-anchored bolts under shear displacement. (δ: Radial clearance).

To further investigate the interaction between bolt deformation and rock joints mechanics, the correspondence between the bolt rotation angle and the shear strength is plotted in Figure 11a. The fitted curve exhibits an inflection point at approximately 50°. When the rotation angle is less than 50°,

 doi:10.20944/preprints202606.0283.v1

the shear strength increases proportionally with the angle. However, once the angle exceeds 50°, the shear strength stabilizes at approximately 0.975 MPa, indicating that the bolt has entered the yielding stage. Similarly, the relationship between the rotation angle and the plastic hinge spacing is shown in Figure 11b. A clear inverse relationship is observed: as the rotation angle increases, the spacing between the plastic hinges decreases. Consequently, a smaller plastic hinge spacing corresponds to a larger rotation angle, which in turn results in a higher shear strength of the rock joints.

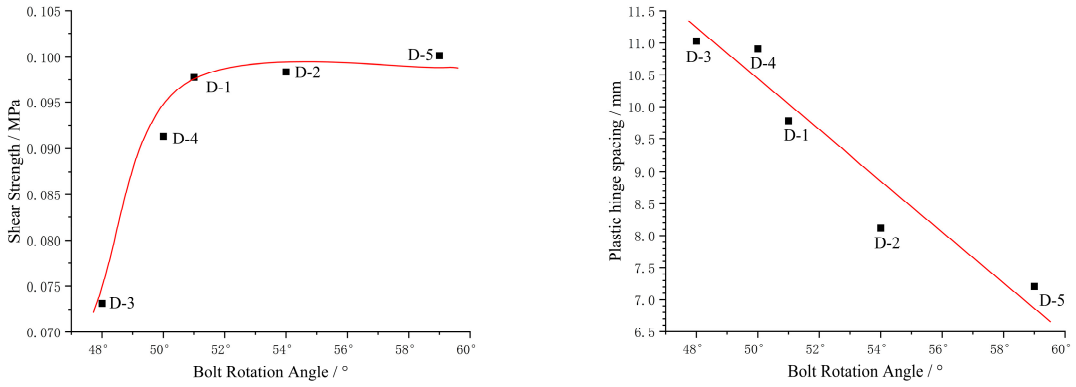

Figure 11. Relationship between bolt rotation angle and mechanical properties: (a) shear strength, and (b) plastic hinge spacing.

3.4. Evolution Law of Shear Strength in Rock Joints

The preceding analysis revealed distinct shear stress responses: the fully grouted specimens exhibited a three-stage curve, while the end-anchored specimens displayed a two-stage curve. These curves were simplified to illustrate the variation in shear stress under increasing displacement, as shown in Figure 12. Under fully grouted conditions, the slopes of all stages are steeper than those of the end-anchored case, enabling a rapid increase in shear strength at relatively small displacements. Conversely, although the end-anchored configuration provides a lower rate of strength enhancement, it offers superior ductility. After reaching bending yield, the bolt does not fail immediately; instead, it continues to provide resistance against rock joints dislocation even under large shear displacements.

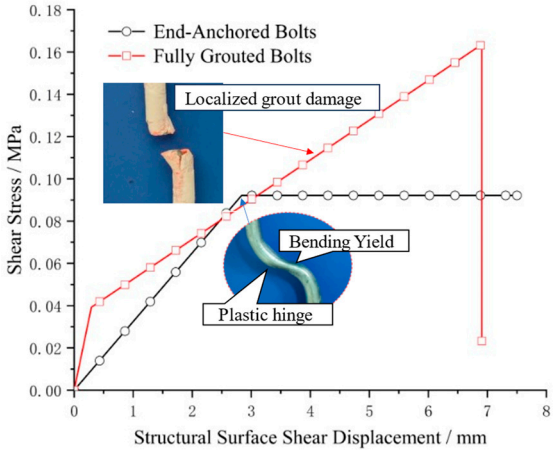

Figure 12. Shear stress-displacement curves of rock joints for end-anchored and fully grouted bolts.

4. Numerical Simulation Analysis of Shear Characteristics in Anchored Rock Joints

4.1. Establishment of the Numerical Model

 doi:10.20944/preprints202606.0283.v1

A complete rock bolting system comprises the bolt body, grout, bearing plate, and nut. Based on the presence of grout filling within the borehole, the bolt is functionally divided into the anchorage segment and the free segment. To investigate the evolution of shear strength in anchored rock joints under various anchorage conditions, a three-dimensional numerical model was developed using FLAC3D 6.0. The rock mass, bolt, and grout were simulated using solid elements. The interactions at the bolt–grout and grout–rock interfaces were captured using interface elements governed by the Coulomb friction law, with the mechanical parameters assigned according to Tables 4–6., a numerical model was developed (Figure 13a). The model simulated the surrounding rock as sandstone, the bolt as HRB335 rebar, the bearing plate as Q235 steel, and the grout as epoxy resin. The rock joints was idealized as a smooth, unfilled discontinuity, with a pre-stress of 150 MPa applied to the bolt.

Table 4. Material properties table.

Material	Bulk Modulus / GPa	Shear Modulus / GPa	Cohesion / MPa	Friction Angle / °	Tensile Strength / MPa	Yield Strength / MPa
Sandstone	15.6	12.7	11	43	5	-
Grout	6.9	5.6	12	30	6	-
Bolt	166.7	76.9	-	-	455	335
Bearing Plate	166.7	76.9	-	-	455	335

Table 5. Mechanical parameters of strain softening model for anchoring agent.

Plastic Shear Strain	0	5e-4	1e-3	5e-2	1e-1
Cohesion / MPa	12	6	1	0.1	0.05
Internal Friction Angle / °	30	30	28	28	28

Table 6. Rock joint related mechanical parameters.

Plastic Shear Strain	Normal Stiffness / (GPa·m^{-1})	Shear Stiffness / (GPa·m^{-1})	Cohesion / MPa	Friction Angle / °
Rock joints I	2,000	2,000	0.1	20
Rock joints II	2,000	2,000	0.1	20
Rock-Grout	9,578	9,578	8	30
Bolt-Grout	9,578	9,578	10	30
Bolt-Plate	21,688	21,688	10	32
Plate-Rock	60,000	60,000	-	-

The application of pre-stress was achieved through a three-step procedure:

1. Model Segmentation: The bolt model was constructed using solid elements. A 10 cm section of the bolt was cut at a distance of 10 cm from the bearing plate.
2. Stress Application: Normal stresses equivalent to the pre-stress magnitude were applied to the exposed ends of the remaining bolt segments. The model was then solved until equilibrium was reached, simulating the pre-tensioning of the bolt.
3. Equilibrium Restoration: The cut bolt element was restored, the mesh was released, and the model was solved again until a new equilibrium state was achieved. This allowed the pre-stress to diffuse throughout the bolt system, as illustrated in Figure 13b.

 doi:10.20944/preprints202606.0283.v1

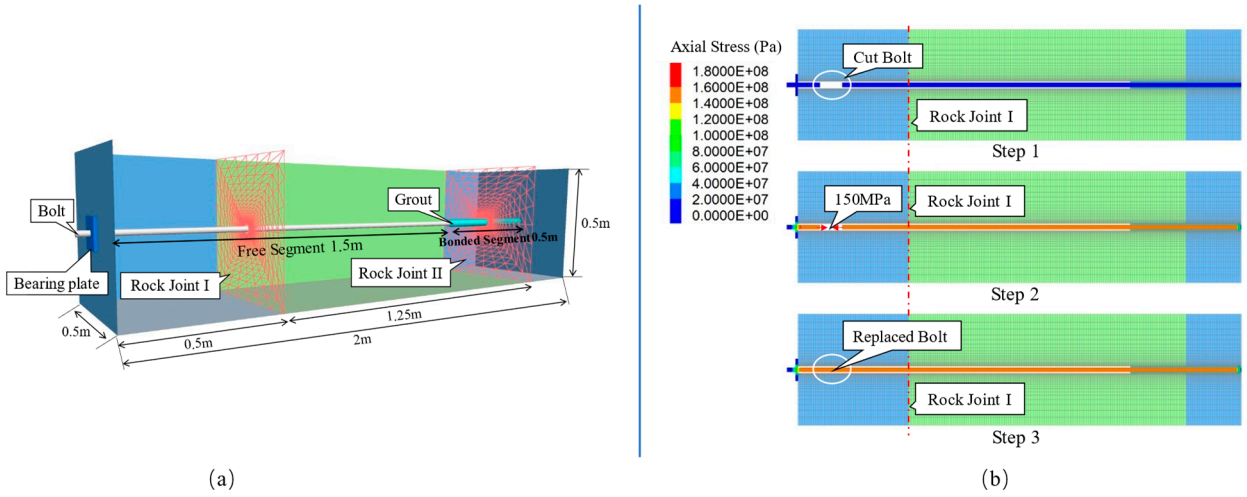

Figure 13. Numerical model for the bolted rock mass with two rock joints and steps for applying prestress. (a) Model setup (b) Prestress application procedure (Steps 1–3).

Displacement loading was applied vertically upward to the regions to the left of rock joints I and rock joints II at a rate of 1 mm per 1000 steps. During the loading process, the damage evolution of the grouting agent and the stress variation of the bolt near the rock joints were monitored. For the grouted segment, the bolt is subjected to a tensile-shear coupled state, and the Von Mises criterion was adopted to determine failure. Loading was terminated when the equivalent stress satisfied $\sqrt{\sigma^2+3\tau^2} \geq \sigma_u$, where σ_u is the ultimate strength of the bolt. For the free segment, failure was judged based on the normal stress of the bolt. When the stress at the plastic hinge satisfied $\sigma_b \geq \sigma_s$, bending yield was considered to have occurred. Here, $\sigma_b = \frac{M_A}{W} + \sigma_A$, where M is the bending moment at the hinge, W is the section modulus, σ_s is the yield strength of the bolt.

4.2. Analysis of Shear Strength Enhancement by Bolt Active and Passive Actions

During the upward displacement loading of the region left of rock joints II, the bolt was considered to have fractured when the average Mises stress across the bolt cross-section at the rock joints reached the ultimate strength of 455 MPa. At this moment, the shear displacement was 4.18 cm, accompanied by an axial stress of 155.40 MPa and a shear stress of 246.98 MPa. The contributions of the axial and shear stresses to the failure were 11.60% and 88.40%, respectively, indicating a shear-dominated tensile-shear coupling failure. The contribution ratio of axial force to shear force is closely related to the damage range of the grout-rock interface. A smaller damage range leads to a higher contribution from shear stress, whereas a larger damage range increases the contribution from axial stress.

With continued dislocation, damage accumulates in the rock mass and grout near the rock joints. As shown in Figure 14a, plastic zones develop in both media; the yellow zone represents rock plasticity, and the blue zone represents grout plasticity. The deformation zone of the bolt coincides closely with the extent of the grout damage. When the bolt reached its ultimate strength, the Mises stress distribution (Figure 14b) revealed that the deformation was primarily concentrated near the rock joints, forming a symmetric S-shape centered on the joint, with a deformation length of 10.84 cm. The Mises stress peaked at the intersection of the bolt and the rock joints and decreased to zero away from the joint. This confirms that the bolt fails in shear preferentially at the rock joints location under shear dislocation.

 doi:10.20944/preprints202606.0283.v1

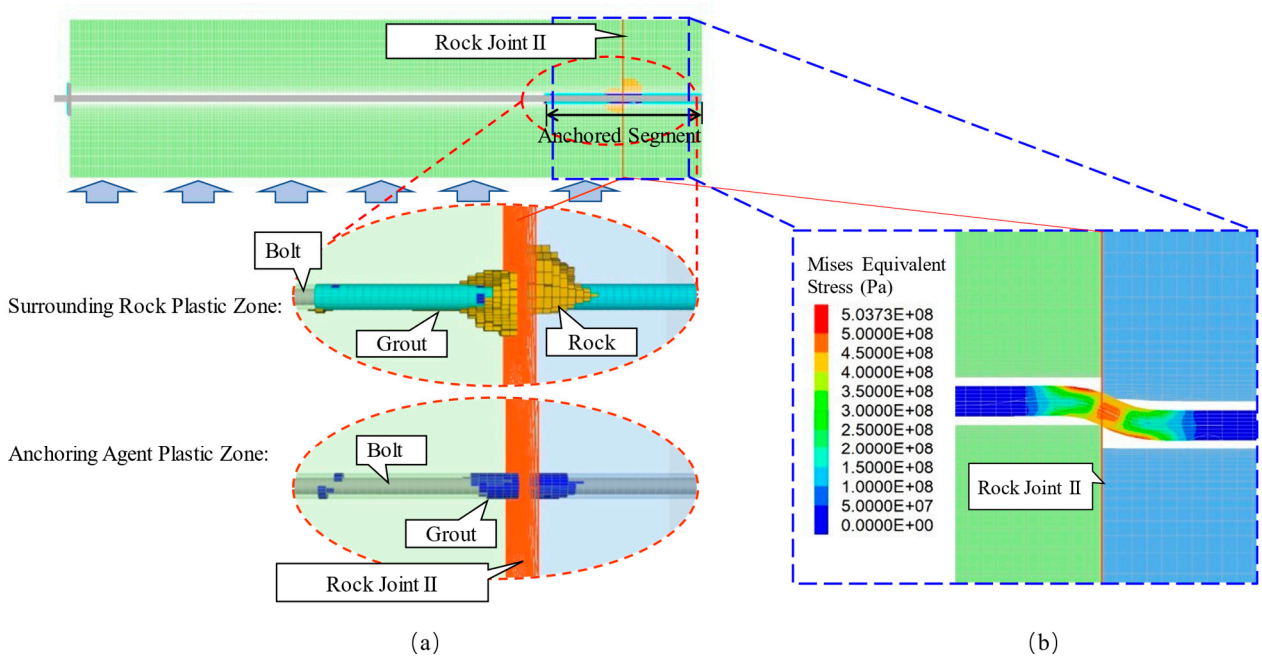

Figure 14. Mechanical response analysis of the bolted rock mass: (a) Plastic zone distribution indicating the interaction between the surrounding rock and the anchoring agent; (b) Mises equivalent stress distribution highlighting stress concentration at the bolt-grout interface.

Upward displacement loading was applied to the region left of rock joint I to simulate two scenarios: without pre-stress and with pre-stress. Without pre-stress, the bolt yielded in bending and formed a plastic hinge when the shear displacement reached 2.41 cm. The bolt eventually fractured when the displacement increased to 11.45 cm. Conversely, with a pre-stress applied, bending yield occurred at a smaller displacement of 1.63 cm. The axial stress distribution along the bolt length (Figure 15) showed that the stress peaked near the rock joints, reaching a maximum of 234.54 MPa. Under the pre-stressed condition, the bolt fractured at a displacement of 5.23 cm.

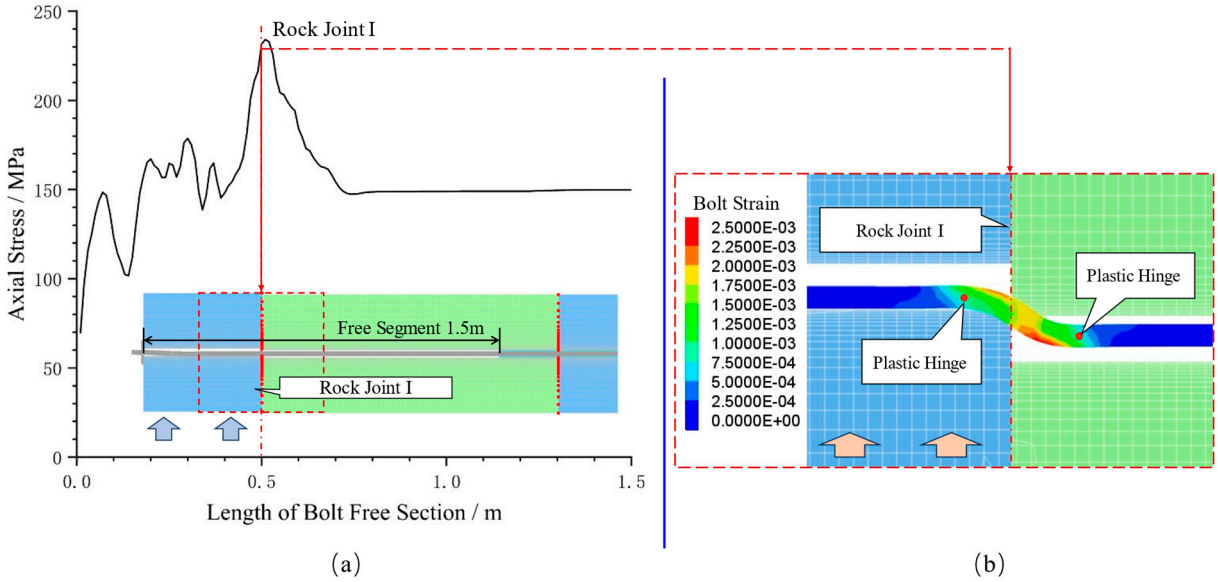

Figure 15. Mechanical response of the bolt under shear loading: (a) Axial stress distribution along the free section. (b) Axial strain distribution indicating the development of plastic hinges at the joint interface.

 doi:10.20944/preprints202606.0283.v1

The average displacement and contact stress of the interface nodes were statistically analyzed. The variation in shear stress with rock joints dislocation is shown in Figure 16. For the grouted segment, the bolt fractured in tensile-shear coupling when the shear displacement reached 4.18 cm, enhancing the shear strength by 0.8024 MPa. For the free segment, the bolt yielded in bending at a displacement of 2.41 cm, providing a strength enhancement of 0.6433 MPa. The numerical curves exhibit a consistent trend with those obtained from the laboratory tests. For the pre-stressed bolt, bending yield occurred at a displacement of 1.63 cm, with the shear strength increasing by 0.8095 MPa. In this case, the pre-tensioning force contributed 0.5634 MPa, while the passive bolt action contributed 0.2461 MPa, accounting for 30.40% of the total strength enhancement.

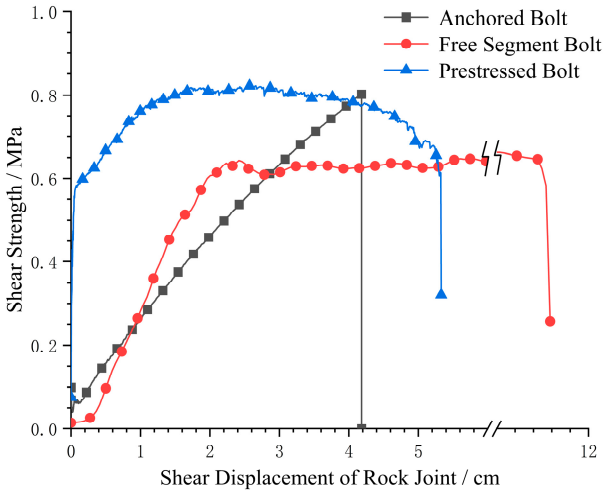

Figure 16. Comparison of shear stress variation curves of the rock joint under different anchorage conditions from numerical simulation.

5. Discussion

The abrupt fluctuations observed in the shear stress curves (Figures 6 and 8) are attributed to the rotation of the rock joints induced by bolt deformation. Although horizontal constraints were applied, the tilting of the specimen altered the angle between the loading platens (Figure 17), leading to sudden variations in the normal stress perpendicular to the rock joints and causing mutations in the shear stress curves. Ideally, the RLJW-2000 testing machine utilizes servo control to maintain constant horizontal stress. However, in practice, the angular misalignment between the horizontal platens resulting from the specimen's tilt significantly affected the normal stress during shear displacement. Consequently, maintaining a strictly constant normal stress throughout the test proved challenging.

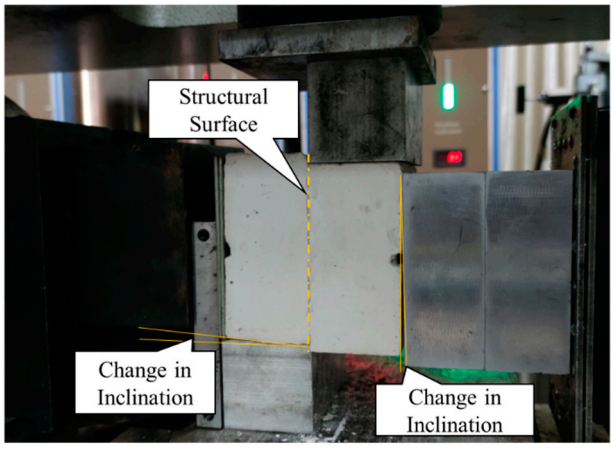

Figure 17. Experimental setup showing the evolution of the inclination angle during the loading process.

 doi:10.20944/preprints202606.0283.v1

6. Conclusions

1. The reinforcement effect of rock bolts on rock joints can be categorized into active action, which suppresses early-stage dislocation through prestress, and passive action, which enhances shear resistance progressively with increasing displacement. Their synergy significantly improves the overall shear capacity of jointed rock masses.

2. The failure mode and strength evolution are strongly dependent on the anchorage type and the damage extent of the grout–rock interface. When the damage zone is smaller than approximately 5 times the bolt diameter, tensile–shear fracture dominates; otherwise, plastic hinges form and bending yield prevails. Fully grouted bolts achieve peak strength rapidly at small displacements, whereas end-anchored bolts sustain resistance under large deformations.

3. In prestressed systems, the active contribution accounts for approximately 69.6% of the total shear strength enhancement, with the passive contribution at about 30.4%. For engineering applications involving high geostress or large potential deformations, end-anchored or yielding bolts are recommended to exploit the large-deformation bearing capacity of passive action. Conversely, where strict control of early-stage deformation is required, priority should be given to prestressed bolts to maximize active support efficiency.

Author Contributions: Conceptualization Y.T. and T.W.; Methodology, Y.T.; Software, Y.T.; Validation, Y.M. and Y.W.; Formal analysis, Y.T.; Investigation, Y.M. and Y.W.; Resources, T.W.; Data curation, Y.T.; Writing—original draft preparation, Y.T.; Writing—review and editing, T.W.; Visualization, Y.T.; Supervision, T.W.; Project administration, Y.T.; Funding acquisition, Y.T. All authors have read and agreed to the published version of the manuscript.

Funding: This research was funded by the Ningxia Education Department Scientific Research Project of Higher Education Institutions, grant number NYG2024251.

Institutional Review Board Statement: Not applicable.

Informed Consent Statement: Not applicable.

Data Availability Statement: The data associated with this research are available and can be obtained by contacting the corresponding author.

Acknowledgments: We thank the Ningxia Education Department Scientific Research Project of Higher Education Institutions (Grant No. NYG2024251) for its financial support. We also thank the academic editors and anonymous reviewers for their kind suggestions and valuable comments.

Conflicts of Interest: The authors declare no conflict of interest.

References

1. Lu, S.L. *Anchoring Force and Anchoring Technology of Bolts*; China Coal Industry Publishing House: Beijing, China, 1998.
2. Kang, H.P. Seventy years development and prospects of strata control technologies for coal mine roadways in China. *Chin. J. Rock Mech. Eng.***2021**, *40*, 1–30.
3. Kang, H.P.; Gao, F.Q.; Wang, X.Q.; Chen, D.D.; Meng, F.L. Development and experimental validation of a test system for simulation of fault-slip rock bursts in coal mine roadways. *J. China Coal Soc.***2024**, *49*, 3701–3710.
4. Xia, C.C.; Sun, Z.Q. *Engineering Jointed Rock Mass Mechanics*; Tongji University Press: Shanghai, China, 2002.
5. Zhong, Z.; Chen, Z.Y.; Hu, Y.J.; Li, S. Shear strength evolution and instability criterion of rough rock joint under variable shear rates. *Chin. J. Rock Mech. Eng.***2025**, *44*, 2592–2607.
6. Liu, C.H.; Li, Y.Z. Research progress in bolting mechanism and theories of fully grouted bolts in jointed rock masses. *Chin. J. Rock Mech. Eng.***2018**, *37*, 1856–1872.
7. Tang, Y.F.; Jiang, D.H.; Wang, T.X.; Ma, Y.X.; Wang, Y.L. Research on the mechanism of the passive reinforcement of rock joint shear strength by bolts under rock joint dislocation. *Appl. Sci.***2023**, *13*, 543.

 doi:10.20944/preprints202606.0283.v1

8. Ge, X.R.; Liu, J.W. Study on shear behavior of bolted rock joints. *Chin. J. Geotech. Eng.***1988**, *10*, 8–19.
9. Ferrero, A.M. The shear strength of reinforced rock joints. *Int. J. Rock Mech. Min. Sci. Geomech. Abstr.***1995**, *32*, 595–605.
10. Teng, J.Y.; Zhang, Y.N.; Tang, J.X.; Zhou, K.P. Study on mechanical properties of anchored layered rock under uniaxial compression. *Rock Soil Mech.***2017**, *38*, 1974–1982+1998.
11. Liu, Q.S.; Lei, G.F.; Peng, X.X.; Wu, X.J. Shear mechanical properties of anchored white sandstone, marble and granite. *Chin. J. Rock Mech. Eng.***2018**, *37*, 4007–4015.
12. Liu, Q.S.; Lei, G.F.; Peng, X.X.; Wu, X.J. Experimental study and mechanism analysis of the influence of bolt anchorage on shear behavior of jointed rock mass. *Rock Soil Mech.***2017**, *38*, 27–35.
13. Si, L.P. Experimental study on mechanical properties of bolts under tensile and shear loads. *J. Min. Strata Control Eng.***2022**, *4*, 18–27.
14. Zhao, Z.H.; Du, J.Z.; Ma, Q.; Liu, J. Analysis of the comprehensive influence of support timing and support parameters on the full section anchors of weakly cemented roadway surrounding rock. *China Min. Mag.***2025**, *34*, 134–144.
15. Yang, H.W. Stress distribution law and support optimization of surrounding rock in large buried trapezoidal roadway. *China Min. Mag.***2023**, *32*, 128–135.
16. Li, W.T.; Yang, N.; Li, T.C.; Chen, W.Z. Implementation and application of bolt fracture failure in FLAC3D. *Chin. J. Rock Mech. Eng.***2016**, *35*, 753–767.
17. Li, X.W.; Yang, G.Y.; Nemcik, J.; Mirza, A.A. Numerical investigation of the shear behaviour of a cable bolt in single shear test. *Tunn. Undergr. Space Technol.***2019**, *84*, 227–236.
18. Zhang, Z.Q.; Liu, Y.; Zhao, Z.T.; Zhang, J.K. Numerical implementation and application of bolt shear fracture in FLAC3D. *China Railw. Sci.***2019**, *40*, 59–68.
19. He, L.L. Implementation and application of bolt tensile-shear fracture in FLAC3D. *Mod. Tunn. Technol.***2021**, *58*, 60–69.
20. Luan, H.J.; Cao, Y.W.; Jiang, Y.J.; Chen, X.G. Implementation and application of bolt tensile-shear coupling failure mode in FLAC3D. *J. Min. Strata Control Eng.***2022**, *4*, 5–15.